DOI: 10.13009/EUCASS2025-716
11TH EUROPEAN CONFERENCE FOR AERONAUTICS AND SPACE SCIENCES (EUCASS)

THERMITE-FOR-DEMISE (T4D): THERMITE CHARGE SHAPING ADVANCEMENTS

Alessandro FINAZZI,[1] *Carlo ZANARDI,*[1] *Oscar PRATOLA,*[1] *Jacopo DOMASCHIO,*[1]
Antonio M. GRANDE,[1] *Francesco PANERAI,*[2] *Stefania CARLOTTI,*[1] *Christian PARAVAN,*[1] *and Filippo MAGGI*[1]

[1]*Dept. of Aerospace Science and Technology, Politecnico di Milano, Milan, Italy*
[2]*Dept. of Aerospace Engineering, The Grainger College of Engineering, University of Illinois at Urbana-Champaign,* Urbana, Illinois, USA

filippo.maggi@polimi.it · www.polimi.it

Abstract

The use of thermite-based materials to aid spacecraft demise during re-entry is currently under investigation as part of EIC THREAD project. In this work, the production of sintered aluminum/iron oxide thermite samples via press-and-sinter method is explored. Pellets were uniaxially compressed and sintered in high-vacuum at 600 °C for 120 minutes. The samples were characterized by optical microscopy, dimension analysis, and compression tests. Despite minimal shrinkage, the formation of necks between aluminum particles and increased ductility suggest that the process is feasible. The presence of iron oxide induced a more brittle behavior upon compression. This effect could be mitigated by limiting the difference in particle size of the two powders.

1. Background

The population of inoperative, man-made objects in Earth orbits, known as space debris, has been increasing at an alarming pace during recent years [1, 2], posing a threat to sustainable space exploration. Such objects are hazards for active missions, as they increase the risk of collisions (the so-called Kessler syndrome [3]). Currently, Low Earth Orbit (LEO) is the most crowded region. The newest regulations prescribe that a spacecraft shall be removed from LEO within five years from the end of its operational life [4, 5]. This is usually accomplished by atmospheric re-entry, requiring reliable decommissioning strategies that guarantee complete demise and minimize casualty risk on the ground. While a possible solution is to adopt a controlled re-entry strategy (*e.g.*, directing the spacecraft towards an uninhabited area through a final, high-thrust maneuver), there are several disadvantages associated to this strategy, including the need for extra propellant and the risks of extra-maneuver that add a potential point-of-failure [6]. The need for effective demise motivates investigation into alternative passive solutions that enable uncontrolled and safe re-entry.

Design-for-Demise (D4D) is the intentional design of a spacecraft to facilitate its complete destruction during atmospheric re-entry. The goal of D4D is to minimize the casualty risk while avoiding a controlled high-thrust maneuver to steer the spacecraft towards an uninhabited area [7]. The European Space Agency (ESA) has adopted D4D as the preferred disposal method for LEO missions [5]. To date, the D4D technique portfolio is strongly heterogeneous: it includes solutions leveraging diverse physical concepts and characterized by different Technology Readiness Level (TRL) [7].

Thermite-for-Demise (T4D) is an avant-garde D4D technique which aims at exploiting the highly exothermic reaction of a thermite charge to facilitate the demise of a spacecraft during atmospheric re-entry [8]. Thermites are extremely energy-dense materials composed of a metal and a metal-oxide mixture, which undergoes a redox reaction when appropriately triggered. They find wide use in a variety of industrial applications, including railroad track welding, underwater cutting torches, pyrotechnic devices, and more [9–11], due to their high adiabatic flame temperature, their relative insensitivity to external stimuli, and the possibility of adjusting their composition to the intended purpose [12]. The rationale behind T4D is to strategically embed thermite charges into spacecraft components to increase the available enthalpy of ablation, perforate the external structure, and induce controlled fragmentation [13, 14]. Although the concept has been validated by different wind tunnel test campaigns [8, 15–17], the technology is still in its infancy (TRL < 3-4). These past experiments have been carried out on thermite in the form of either free-flowing

DOI: 10.13009/EUCASS2025-716

powder or pellets, that need to be contained due to their inability of maintaining a defined shape. Associated shortcomings include the risk of contamination of nearby equipment, limited heat transfer to the structure to be demised, and the risk of uncontrolled fragmentation of the vessel containing the thermite due to an excessive pressure build-up upon reaction. Therefore, it is necessary to investigate new approaches to address these limitations.

An innovative solution resides in the use of Multifunctional Energetic Materials (MFEMs). MFEMs are a class of materials which combine high energy density with at least one other desired property that can be exploited in an engineering application [18]. Mechanical strength is the functionality that is often sought after. In this case, MFEMs are also referred to as Structural Reactive Materials (SRMs). A comprehensive overview on SRMs can be found in the work of Hastings and Dreizin [19]. It has been shown that thermites can be shaped into specific geometries by embedding the powder into a paste that can be extruded by a 3D printer [20], similarly to what is done with cementitious materials [21]. The 3D printed material retains its reactive properties and can transfer heat to the designated target without the need of fixtures to hold the exothermic material in place during the reaction. However, the cement-like compounds seems to be poorly suited for space applications. The possibility of manufacturing thermite charges capable of maintaining their shape throughout a spacecraft's life-cycle and/or of bearing a structural load has yet to be thoroughly explored.

This work presents recent advancements towards the shaping of thermite charges by means of metal sintering. Section 2 reports a discussion of the sintering technology applicability to thermite powders, while in Section 3 the materials and the methods used in this investigation are presented. Section 4 provides the results obtained and a critical discussion thereof. Finally, the main conclusions of this work are provided in Section 5.

2. Sintering technology applicability to thermites

The press-and-sinter method is a widely used powder metallurgy (P/M) technique to obtain net or near net shape solid parts from metal powders. The pressing phase allows to give the powder a specific geometry and to obtain what is referred to as "green compact" (or just "green"). Compaction is achieved by a punch and die apparatus. A given amount of powder is poured into the die and punch-pressed to the desired geometry. The pressure ranges from 70 to 800 MPa for most industrial applications, depending on the material, the geometry, the desired level of compaction, and the mechanical limits of the die. The powder can be mixed with a lubricant to mitigate friction, allow a smooth flow of the particles, and therefore reduce the pressure requirement. Examples of lubricants are stearic acid, paraffin wax, and PTFE sprays, but also common penetrating fluids [22]. During pressing, the apparent density of the powder increases up to a fraction of the Theoretical Maximum Density (TMD) of the material, with voids and cavities filling the inter-particle volume. Excessive pressure could fracture the powder particles by exceeding their ultimate compressive stress. Usually, once a certain pressure threshold is exceeded, a region of diminishing returns is reached without appreciable increase in green compaction [23]. At the same time, excessively low initial compaction could lead to poor sintering results. Pressure can be applied on one or both sides of the mold (single vs. double ended pressing), influencing the gradient of compaction experienced by the green. Double ended compression is preferable due to improved uniformity. Greens usually have enough structural strength to maintain their shape and to resist gentle handling [24].

During the sintering process, the green is placed inside a furnace, where temperature is raised and held for a certain period of time. The furnace can be controlled both in temperature and atmosphere. Sintering can occur in a reactive atmosphere (*e.g.*, nitrogen or hydrogen), inert atmospheres, or vacuum. Heating is usually a two-step process: first, a target temperature is reached, under a protective atmosphere, to remove any possible binder/lubricant used during the pressing phase; then, the temperature is raised and maintained slightly below the melting temperature of the metal powder, usually in the 70-90% range [25]. The sintering time depends on the composition. The heating rate is also a critical parameter to control, as a too steep one can lead to cracking and defects. During sintering, different bonding processes occur between the particles, effectively leading to the elimination of the structure of the individual particles and the solidification of the green. The main bonding mechanism is thought to be diffusion, but other processes like liquid and vapor phase material transport may also contribute to solidification [26]. As bonding by diffusion occurs between two particles, the distance between them is shortened. For this reason, shrinkage is usually observed as a result of sintering.

In this work, thermite consolidation via sintering is explored. While sintered thermites through press-and-sinter method were never reported previously, similarities with Metal Matrix Composites (MMCs) [27] can be recognized. This class of materials is produced via metal-additive sintering, which can effectively consolidate structural integrity of the final product. During the sintering process, the additive can be considered inert and its main effect is to hinder diffusion. The inclusion of additives allows for the tuning of certain effective properties, like stiffness, wear resistance, and thermal expansion coefficient. When dealing with sintering, a thermite can be seen as a composite metal material, where the matrix is the metal fuel (*e.g.*, aluminum powder), and the additive is the metal oxide (*e.g.*, hematite). The only available reference of attempts at sintering thermite were performed on a thermite mixture of tantalum and tungsten oxide through spark plasma sintering [28]. No attempts at sintering according to classical P/M were found.

DOI: 10.13009/EUCASS2025-716

The process of creating a thermite-based sintered MMC presents many different variables. The most important is the weight/volume fraction of the two components: it affects the stoichiometry of the thermite, changing the oxidizer to fuel (O/F) ratio, and the effectiveness of the sintering process, by introducing more particles that do not participate in the consolidation. A ∼30% limit on the volume fraction of the additive was identified as the ceiling to maintain effective sintering [27]. The particle size distribution of the powders plays a key role in the reactivity of the starting composition [29]. The reactivity of the mixture has to be controlled, in order to avoid premature ignition of the thermite during sintering. Particle size distribution is also particularly important for the metal matrix itself, since it influences the initial filling factor and the densification mechanics, and therefore the effectiveness of the sintering process [27]. When selecting powders for MMCs, the same particle size is often used both for the matrix and the additive, since it produces better distribution of the additive inside the matrix [30]. The same principle has been adopted throughout many examples in the literature [31, 32].

In this work, aluminum is sintered to explore thermite-based MMC. Two aspects should be considered in this process. Firstly, reactive metals such as pure aluminum tend to stick to other metals [33] in a phenomenon called "galling". This results into a strong bond of the aluminum to the die walls, ruining the quality of the green. Abundant use of lubrication can prevent this phenomenon by creating a film between the metal particles and the steel. Secondly, the choice of the sintering atmosphere has to be carefully evaluated, since aluminum is subject to oxidation. Some reactive atmospheres, like nitrogen, are reported to be beneficial for aluminum sintering. Others, like hydrogen, significantly impede the sintering process. Inert atmospheres, while protecting the sample from oxidation, slightly hinder the sintering process. High vacuum is a valid condition where sintering can be performed, and it eliminates the drawbacks of some of the other atmospheres [34].

In order to assess if a sample was successfully sintered, the simplest approach is to measure its physical properties. As reported in [35, 36], one of the main indicators for sintering is densification. A shrinkage of all dimensions should be appreciable, since all the particles should have isotropically bonded with their neighboring ones by creating "necks", hence transferring some material by diffusion, filling the space between the particles. Formation of necks manifests as a decrease in distance between the particles' centroids, leading to a bulk shrinkage. The extent of this effect depends on the degree of compaction obtained during the pressing phase.

Analyses on the mechanical properties of the sample can also indicate whether it was successfully sintered or not. In fact, newly pressed greens are fragile and could break or lose material just by rough handling. Green cylindrical pellets subject to compression tend to undergo brittle failure, forming the typical hourglass shape of brittle materials. Conversely, a sintered sample is expected to behave like a solid metal part. For instance, it will not easily lose material through handling. Under compression testing, it will undergo ductile deformation typical of metals and it will deform instead of cracking. Metallographic surface analysis of the samples can also reveal if the sample was successfully sintered, as necks created between the metal particles may be observed. Moreover, sintered pieces show greater electrical conductivity, attributed to a decrease in porosity as compared to the unsintered packed powder [37].

3. Materials and methods

3.1 Powders

The powders used for this experiment were pure aluminum, a thermite composite of aluminum and red iron oxide (Fe_2O_3, or hematite), and a second thermite composite of aluminum and black iron oxide (Fe_3O_4, or magnetite). The specifications of the powders are reported in Table 1. Pure aluminum specimens were produced to verify the effectiveness of the adopted sintering procedure in a non-composite powder. Aluminum/iron oxide thermite was chosen as it was used as a reference in previous works [8, 15]. Red iron oxide was reported to transition to black iron oxide before the ignition of the thermite mixture when subjected to slow heating [38]. The same transition is expected to happen during the sintering process, which was explored by sintering tests with Al/Fe_2O_3 thermite. Subsequently, the final thermite pellets were produced directly starting from Fe_3O_4 powder at different mass loadings. The compositions analyzed during this work are presented in Table 2. All the powders were processed using an acoustic mixer to obtain good homogeneity and to break any agglomerate. Both thermite mixtures exhibited an ignition temperature above ∼ 700°C [38, 39], which rules out accidental ignition inside the sintering furnace.

3.2 Pellet Production

The powders were shaped into pellets using the equipment reported in Table 3. The pressure exerted by the press was manually regulated by the operator, with the aid of an analog gauge. The samples were produced using an internal die pressure of 250 MPa, according to the values reported in [23]. All pellets were pressed to a unitary aspect ratio

DOI: 10.13009/EUCASS2025-716

Powders	Manufacturer	Purity	Characteristics	Theoretical Density
Aluminum	AMG Alpoco	≥ 99%	Spherical, 30 μm (D0.5 = 36.30 μm*)	2.71 g/cm^3
Fe_2O_3	Thermo Scientific	98%	-325 mesh (D0.5 = 0.45 μm*)	5.24 g/cm^3
Fe_3O_4	Thermo Scientific	97%	-325 mesh (D0.5 = 1.50 μm*)	5.17 g/cm^3

Table 1: Characteristics of the starting ingredients. *: property measured during this work, using a Malvern Mastersizer 2000 Scirocco.

Composition	Ox. mass fraction [%]	Ox. volume fraction [%]	Theoretical Density [g/cm^3]
Al	0	0.00	2.70
Al + Fe_2O_3	20	11.10	2.99
Al + Fe_3O_4	10	5.50	2.85
	20	11.59	3.00
	30	18.34	3.16

Table 2: Powder compositions.

(length/diameter). Higher aspect ratios were avoided to limit the risk of significant compaction gradients throughout the length of the samples. This translated to a mass of powder of ∼1 g, which was then kept constant throughout all the formulations for consistency. Samples with higher aspect ratio showed poor compaction and were therefore discarded.

Equipment	Manufacturer and Model	Specifications
Hydraulic press	Unicraft WPP 10 TE	max 10 t
Punch and die set	Precision Elements Ltd (PPDS)	8.0 mm internal diameter, D2 tool steel, single action
Lubricant	WD 40 penetrating oil	As per die manufacturer recommendations

Table 3: Green production equipment.

The greens were sintered in a HTSolutions HT-S1 furnace. This equipment allowed the use of specific atmospheres, as well as high vacuum (see Table 4). Initial sintering runs relied on a nitrogen-based atmosphere which, despite achieving sintering, led to the formation of brittle aluminum nitride. This manifested during mechanical tests conducted later. The nitrogen atmosphere should have been beneficial to the sintering of aluminum according to the available literature [34], but it is likely that the extended sintering time used for this campaign was not ideally suited to the use of a reactive atmosphere. For this reason, high vacuum conditions were preferred for the final production campaign. The sintering conditions were the following:

- Temperature: ∼10°C/min ramp up to 600°C. Temperature was kept constant for 120 minutes. At the end of the heating cycle, the heater was turned off and cooling was allowed to happen naturally with unrestricted rate. The temperature profile is shown in Figure 1.
- Atmosphere: the sintering was performed under high-vacuum (< 10^{-6} bar). After cool-down, mild vacuum was kept while waiting for an operator to unload the furnace.

Equipment	Manufacturer and Model	Specifications
Sintering furnace	HTSolutions, HT-S1	1400°C, controlled atmosphere from ∼ 10^{-6} bar to 4 bar
Sample holder	LLF	Alumina, 90x60x20 mm

Table 4: Sintering equipment.

3.3 Sample optical observation

Samples produced by pressing and sintering were observed through an optical microscope (Nikon Eclipse 80i) to assess diffusion bonding between the aluminum particles. The specimens were encased inside appropriate cold mounting resin (QPREP QPOX 92 from QATM/Verder Scientific). The pellets were prepared inside silicon molds, the resin was thoroughly weighted, mixed, and de-gassed using a vacuum pump. The resin was then cast inside the molds until full coverage. The full molds were transferred to a vacuum chamber to de-gas the porosity of the pellets and allow the resin

DOI: 10.13009/EUCASS2025-716

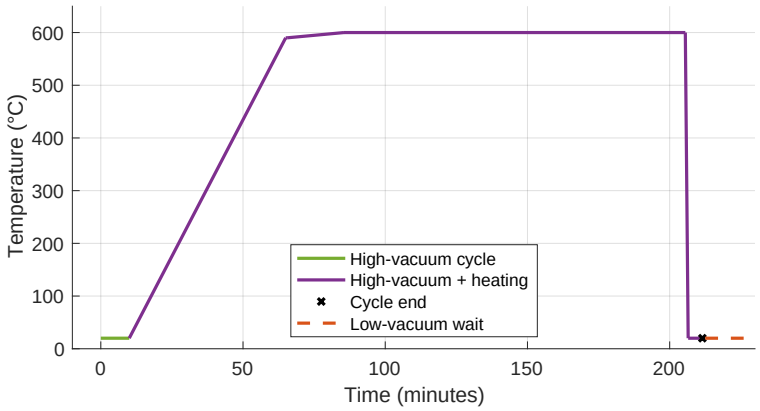

Figure 1: Furnace temperature and vacuum profile.

to fully penetrate and stabilize them through several cycles of vacuum and atmospheric pressure. This step is especially important to stabilize the green pellets, which naturally lack any type of adhesion between the particles. The resulting resin blocks were then progressively sanded with increasing grit abrasives, to expose the structure below the surface. The last preparatory step was lapping with the aid of a polishing compound.

3.4 Mechanical characterization

The dimensions of all the sintered samples were compared before and after the sintering process to verify the presence of shrinkage, which indicates successful sintering. The measurements were taken with a digital micrometer with a 1 μm resolution. Three measurements for the diameter were taken and averaged to compensate for errors due to pellet irregularity.

Compression tests were performed on a universal testing machine (MTS mod. 810) at a displacement rate of 1 mm/minute. Three sintered and three green pellets were tested for each composition. The yield strength and Young modulus were computed from the stress-strain curves according to the standard ASTM E9-19 on compression testing of metallic materials at room temperature [40]. The displacement was measured with an extensometer (MTS mod. 634.31F-24) applied to a custom jig that was built to replicate the movement of the pressing faces, since it was impossible to apply the instrument directly to the specimens due to their small dimensions (see Figure 2). The same test was carried out on three pellets machined from a solid aeronautical grade aluminum alloy billet, with identical dimensions to the sintered ones, used as a reference standard.

The experiments follow the ASTM E9-19 standard, except for two modifications. First, pellets were pressed to an aspect ratio equal to 1, versus a value above 2 prescribed by the standard. Second, the standard prescribes the use of hardened and surface ground steel plates to interface with the specimen being tested, as well as the use of lubricants. This is suggested to prevent the pellets' faces from being constrained by friction, thereby creating non-uniaxial stresses. However, this equipment was not available at the time of testing, and an off-the-shelf steel plate was used as a pressing surface, without any special lubricant or treatment. The main consequence of this was a significant barreling effect on the samples. For this reason, the results are presented as a relative grading between the thermite pellets and the machined pellets.

4. Results and discussion

4.1 Optical observation

Optical examination of the Al/Fe_2O_3 thermite pellets highlights a pronounced color shift of the finer powder after the sintering process (see Figure 3). The shift from red to black strongly suggests that the slow heating inside the furnace caused the oxide transition to Fe_3O_4, analogous to what is documented in [38]. Moreover, unlike Al/Fe_2O_3 thermite, the sintered samples presented ferromagnetic properties. Following these observations, Fe_2O_3 was discarded in favor of Fe_3O_4 as starting ingredient for all other characterizations.

The microscope images of Al and Al/Fe_3O_4 thermite pellets, before and after sintering, are reported in Figure 4 and Figure 5. The comparison between the green and the sintered samples highlights appreciable differences. A much smoother surface was achievable for the sintered pellets, while the greens, despite the epoxy resin stabilization, show

DOI: 10.13009/EUCASS2025-716

Figure 2: Compression test jig in use.

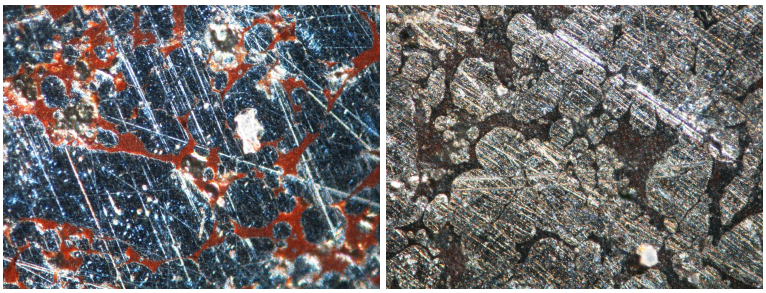

(a) Green Al/Fe_2O_3 (b) Sintered Al/Fe_2O_3

Figure 3: Color shift of Fe_2O_3 after sintering, which can be attributed to the transition to Fe_3O_4.

holes due to the detachment of particles during polishing. In the case of pure aluminum sintered pellets, the particles exhibit bridging and bonding at the contact points, creating necks. This result is a favorable evidence for the quality of the sintering. The pellets containing the iron oxide, on the other hand, show larger and more pronounced boundaries between the aluminum particles. This is attributed due to the presence of very fine iron oxide particles that filled some of the interstitial spaces between the larger aluminum ones. A pronounced segregation phenomenon is also apparent in the case of sintered Al/Fe_3O_4: the iron oxide particles formed large agglomerates. This behavior may be due to the use of different size particles between the matrix and the additive, resulting in poor homogeneity and limited diffusion bonding when compared to pure aluminum.

4.2 Dimensional analysis

Dimensional data of the sintered pellets is reported in Table 5. Pure aluminum showed negligible shrinkage. This may be due to the already high level of compaction reached during the pressing phase. In fact, even without significant shrinkage, the final density of the sintered samples is 91.5% of the TMD. As the concentration of iron oxide is increased, the shrinkage effect is more noticeable, albeit still below 1%. This is likely due to the higher initial porosity of the samples loaded with iron oxide. Therefore, the greater densification that is observed is attributed to the lower initial compaction, rather than to a better bonding of the aluminum particles. Overall, samples with higher percentage of iron oxide are less dense, when compared to their respective TMD.

Moreover, it was observed that all sintered specimens are electrically conductive, whereas their green counterparts are very poor conductors. This suggests that, despite the limited densification and iron oxide segregation, aluminum necks have formed across all the sintered pieces, effectively enhancing their conductivity. Indeed, an increase in electrical conductivity after successful sintering is well known (*e.g.*, [37]).

4.3 Compression testing

The stress-strain curves resulting from the compression tests are reported in Figure 6. The behavior shown by the processed pellets against their respective greens allows for a preliminary observation of the success of the sintering

DOI: 10.13009/EUCASS2025-716

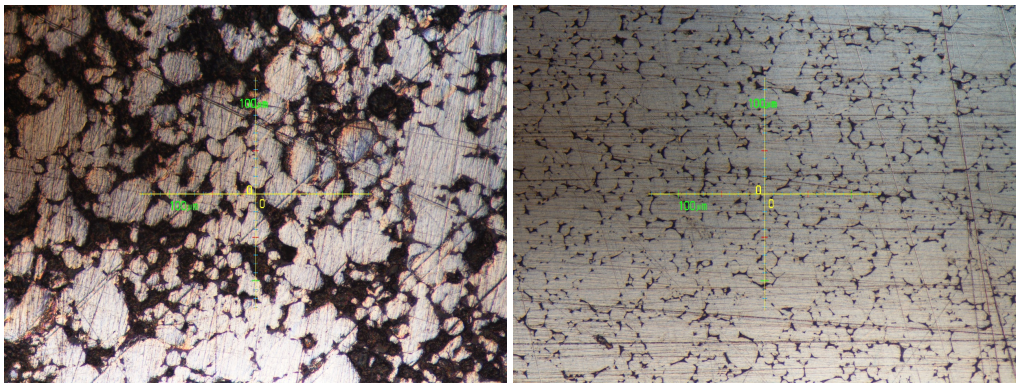

(a) Green Al, 20x magnification (b) Sintered Al, 20x magnification

Figure 4: Optical microscope pictures of 100% Al green and sintered pellets.

Formulation	**Volume change [%]**		**Density change [%]**		**Sintered density [% TMD]**	
	Average	Std. deviation	Average	Std. deviation	Average	Std. deviation
pure Al	0.118	0.092	-0.118	0.092	91.49	0.71
90-10	0.060	0.027	-0.060	0.027	89.84	0.27
80-20	-0.440	0.156	0.443	0.157	85.58	0.46
70-30	-0.484	0.155	0.487	0.156	81.81	0.33

Table 5: Dimensional analysis results of the sintered pellets; positive values indicate an increase of that quantity after sintering. Each value was obtained by averaging over 6 samples. The potential presence of lubricant was neglected in the computation of densities.

process. All the green pellets exhibit a brittle behavior, responding rigidly to compression until sudden failure. The sintered pellets show instead ductile deformation. Pure aluminum and the formulation including 10% Fe_3O_4, in particular, feature an extended plastic region, indicating successful sintering. Increasing the iron oxide content to 20% and 30%, the sintered pieces show similar rigidity to the green pellets. The yield stress, though, is significantly higher, which indicates bonding, albeit poor.

The values of the Young modulus and the yield stress computed for the sintered pellets are reported in Figure 7. All the sintered pellets present a modulus of elasticity ranging from 10% to 20% of that of the reference aeronautical machined sample. Pure aluminum is the stiffest, and the measurement appears to be repeatable across all three samples. The addition of iron oxide lowers the stiffness of the pellets, and introduces more variability in the measurements. The yield stress of the 100% aluminum sintered pellets is roughly 30 MPa, which is in accordance with typical values reported for the virgin material [41]. The iron oxide-loaded samples appear to yield slightly above that value, but with significantly higher uncertainty.

Visual analysis of the pellets after compression testing gives a good representation of their mechanical behavior (Figure 8). The aluminum samples showed good ductility and significant plastic deformation. The barreling effect, due to the low aspect ratio of the pellets, is clearly visible. All the samples loaded with Fe_3O_4 showed a brittle behavior during testing. The lateral surface of the pellets is characterized by fractures and did not deform into a barrel shape like the pure aluminum pellets. The same images suggest a gradient of mechanical properties in the longitudinal direction, possibly due to differences in initial compaction compatible with the single action pressing used during production.

5. Conclusions

This work investigated the possibility to apply the classic press-and-sinter technique to aluminum/iron oxide thermite, with the objective of producing thermite charges capable of maintaining their shape to aid the demise of structural spacecraft components during atmospheric re-entry. A comprehensive literature survey was carried out to identify the critical parameters for the production of sintered pellets, including compaction pressure, sintering temperature, atmosphere, and particle size. A suitable production procedure was developed accordingly. Pellets of pure Al, Al/Fe_2O_3, and Al/Fe_3O_4 thermites were produced. Al/Fe_2O_3 thermite showed signs of oxide transition to Fe_3O_4 during the sintering process, which directed processing efforts towards the latter formulation. The sintered thermite pellets were characterized by optical microscopy, dimensional analysis, and compression testing. Pure aluminum samples showed

DOI: 10.13009/EUCASS2025-716

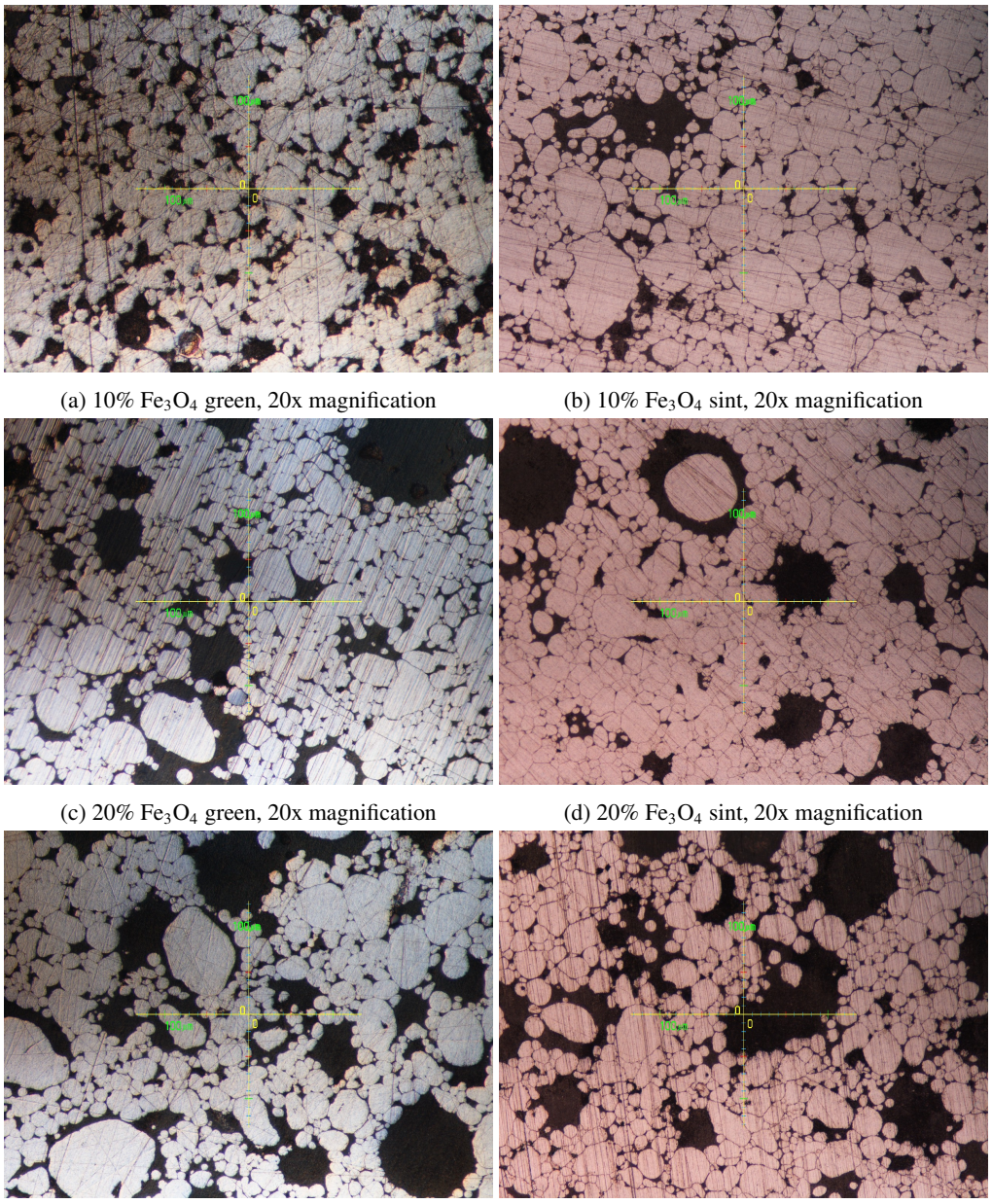

(a) 10% Fe_3O_4 green, 20x magnification

(b) 10% Fe_3O_4 sint, 20x magnification

(c) 20% Fe_3O_4 green, 20x magnification

(d) 20% Fe_3O_4 sint, 20x magnification

(e) 30% Fe_3O_4 green, 20x magnification

(f) 30% Fe_3O_4 sint, 20x magnification

Figure 5: Optical microscope pictures iron oxide loaded green and sintered pellets.

several indicators of successful sintering. These include the formation of necks between the powder's particles, ductile behavior under compression, and increased electrical conductivity. They did not exhibit significant densification, owing to the already high level of compaction achieved during pressing (> 90% TMD). The pellets containing iron oxide were found to be far more brittle than pure aluminum, while showing higher yield strength as compared to their green counterparts. Densification of these samples was scarce, and both green and sintered pellets presented worse compaction than pure aluminum. Microscope images showed that iron oxide caused significant particle segregation, hindering the efficacy of the sinterization. It is suggested that the cause of this behavior resides in the difference in particle size between the two powders.

The exploratory nature of this work provided directions for future developments and improvement. First, the production procedure could benefit by using a double action press to obtain more uniform green pellets, and by tuning the sintering program to the specific thermite formulation. Second, while we focused on the legacy aluminum/iron oxide thermite for T4D studies, other powder compositions and granulometries could lead to improve sintering and are worthy of future investigation. Lastly, a perfected testing procedure would yield improved mechanical characterization.

DOI: 10.13009/EUCASS2025-716

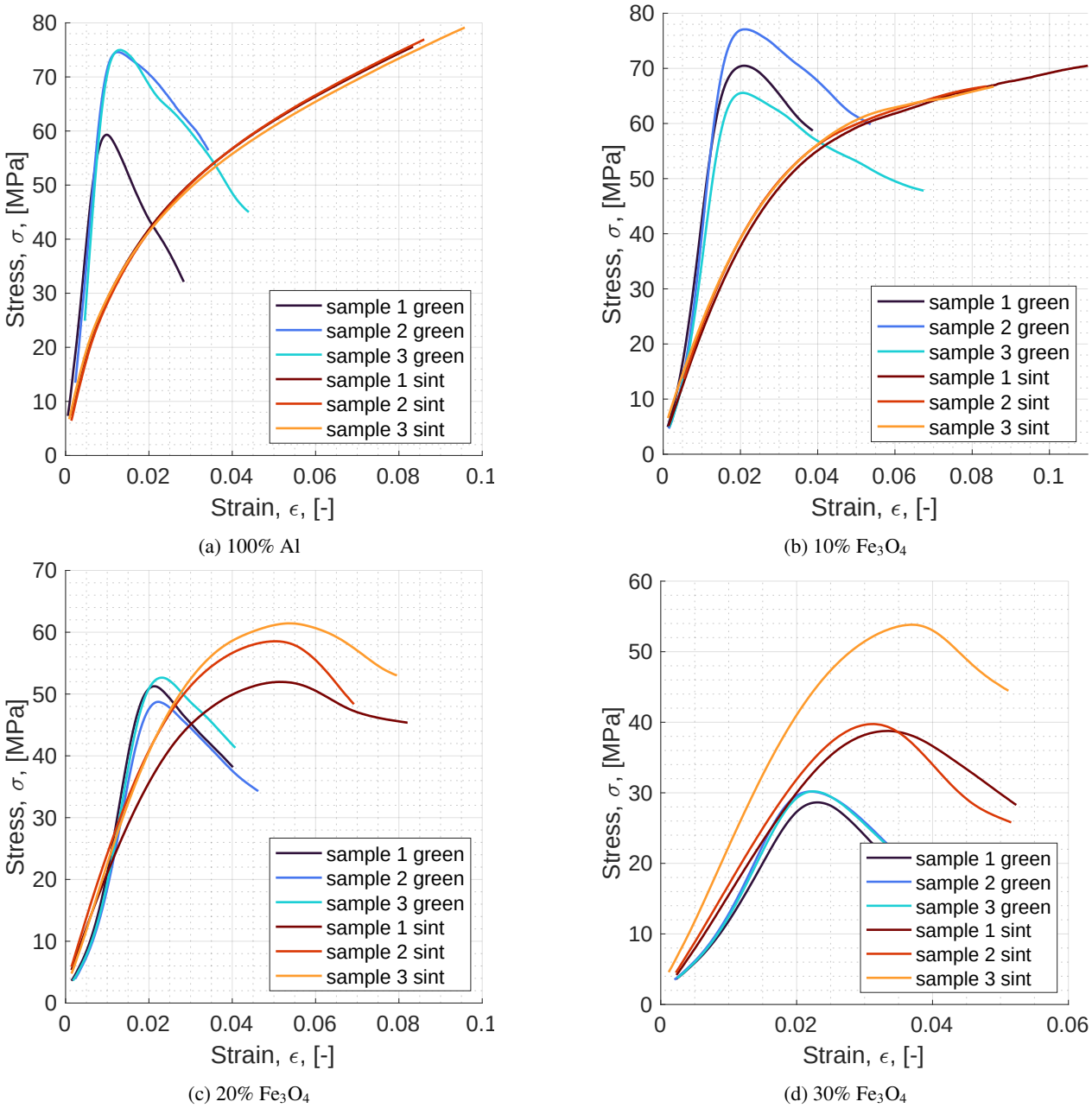

(a) 100% Al

(b) 10% Fe_3O_4

(c) 20% Fe_3O_4

(d) 30% Fe_3O_4

Figure 6: Compression tests stress-displacement curves.

6. Acknowledgments

The authors sincerely thank Mr. Alberto Verga and Mr. Paolo Rubini for their support during the experimental activity.

Funded by the European Union through the European Innovation Council (EIC) within the THREAD project (Grant agreement ID: 101186901). Views and opinions expressed are however those of the authors only and do not necessarily reflect those of the European Union or the European Innovation Council (EIC). Neither the European Union nor the granting authority can be held responsible for them.

European Innovation Council

Funded by the European Union

DOI: 10.13009/EUCASS2025-716

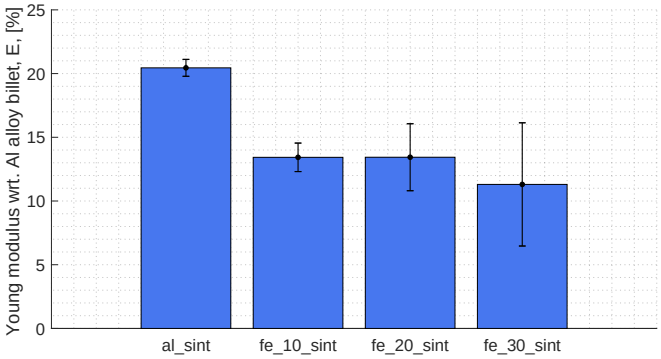

(a) Young modulus as a percentage of the value measured for the reference pellets, machined from aeronautical alloy

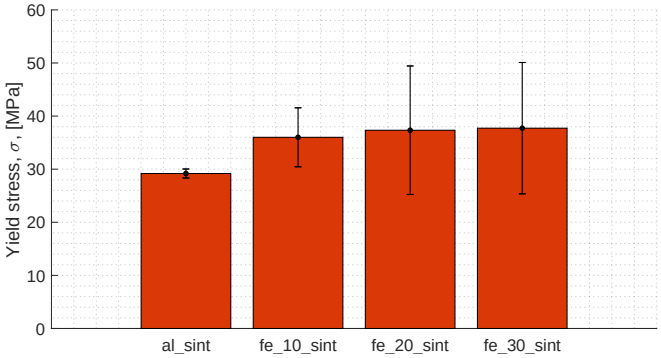

(b) Yield stress

Figure 7: Young modulus and yield stress of sintered Al/Fe_3O_4 thermite pellets.

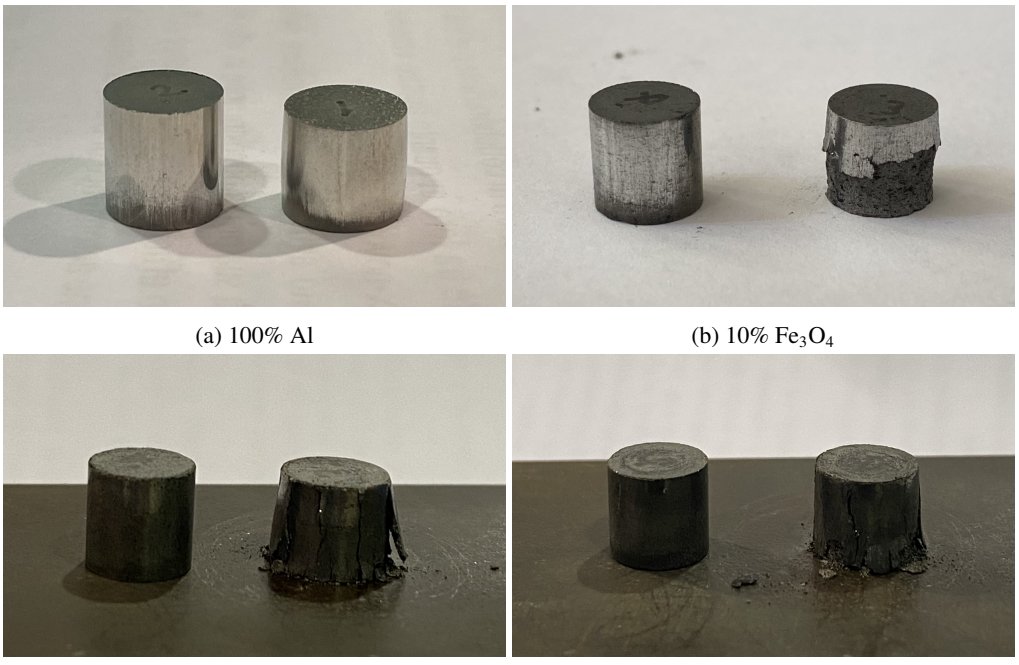

(a) 100% Al

(b) 10% Fe_3O_4

(c) 20% Fe_3O_4

(d) 30% Fe_3O_4

Figure 8: Sintered pellets before (left) and after (right) compression tests.

References

[1] Anon. ESA's Annual Space Environment Report. Technical Report GEN-DB-LOG-00288-OPS-SD, European Space Agency, Darmstadt, Germany, 2025.

DOI: 10.13009/EUCASS2025-716

[2] Anon. IADC Report on the Status of the Space Debris Environment. Technical Report IADC-23-01, Issue 2, Rev. 0, Inter-Agency Space Debris Coordination Committee, 2024.

[3] D.J. Kessler and B.G. Cour-Palais. Collision Frequency of Artificial Satellites: The Creation of a Debris Belt. *Journal of Geophysical Research*, 83(A6):2637–2646, 1978.

[4] Anon. Space Innovation; Mitigation of Orbital Debris in the New Space Age. Technical Report FCC-CIRC2209-01, Federal Communications Commission, 2022.

[5] AA. VV. ESA Space Debris Mitigation Requirements. Technical Report ESSB-ST-U-007, Issue 1, Rev. 0, European Space Agency, 2023.

[6] S. Perrault, T. Soares, and L. Innocenti. Re-entry strategies to comply with space debris mitigation guidelines. In *First International Orbital Debris Conference*, Sugar Land, Texas, USA, 2019.

[7] B.M. Cattani, A. Caiazzo, L. Innocenti, and S. Lemmens. An Overview of Design for Demise Technologies. In *8th European Conference on Space Debris*, Darmstadt, Germany, 2021.

[8] A. Finazzi, D. Daub, F. Maggi, C. Paravan, S. Dossi, T. Lips, G. Smet, and K. Bodjona. Thermite-for-demise (T4D): Experiments and numerical modelling on ball-bearing unit mock-ups containing thermite in an arc-heated wind tunnel. *Acta Astronautica*, 223:550–576, 2024.

[9] M.J.M.M. Steenbergen and R.W. van Bezooijen. *Wheel-rail Interface Handbook*, chapter 12 - Rail welds. Woodhead Publishing in Mechanical Engineering, Cambridge, UK, 2009.

[10] S. Turner. Thermite cutting device, 1997. Patent GB 2312864 A.

[11] J.C. Carter Jr. Portable metal cutting pyrotechnic torch, 2003. Patent US 2003/0145752 A1.

[12] S.H. Fischer and M.C. Grubelich. Theoretical energy release of thermites, intermetallics, and combustible metals. In *24th International Pyrotechnics Seminar*, Monterey, California, USA, 1998.

[13] D. Dilhan and P. Omaly. Élement de véhicule spatial a capacité d'autodestruction ameliorée et procedure de fabrication d'un tel elément, 2011. Patent FR 2975080B1.

[14] R. Seiler and G. Smet. Exothermic reaction aided spacecraft demise during reentry, 2018. Patent EU 3604143A1.

[15] A. Finazzi, D. Daub, F. Maggi, C. Paravan, S. Dossi, T. Lips, G. Smet, and K. Bodjona. Thermite-for-demise (T4D): experiments and numerical modelling on solar array drive mechanism mock-ups containing thermite in an arc-heated wind tunnel. *CEAS Space Journal*, 2025.

[16] K.A. Monogarov, I.N. Melnikov, S.M. Drozdov, D. Dilhan, Yu.V. Frolov, N.V. Muravyev, and A.N. Pivkina. Pyrotechnic approach to space debris destruction: From thermal modeling to hypersonic wind tunnel tests. *Acta Astronautica*, 172:47–55, 2020.

[17] T. Schleutker, A. Gülhan, B. Esser, and T. Lips. ERASD – Exothermic Reaction Aided Spacecraft Demise – Proof of Concept Testing. Technical report, DLR, Supersonic and Hypersonic Technologies Department, 2019.

[18] N.N. Thadhani, R.W. Armstrong, A.E. Gash, and W.H. Wilson. Multifunctional energetic materials. *Materials Research Society Symposium Proceedings*, 896:130–132, 2006.

[19] D.L. Hastings and E.L. Dreizin. Reactive Structural Materials: Preparation and Characterization. *Advanced Engineering Materials*, 20:1700631, 2018.

[20] K.E. Neely, A.M. Strauss, and K.C. Galloway. Additively manufactured reactive material architectures for exothermic brazing. *Additive Manufacturing Letters*, 1:100005, 2021.

[21] C. Gosselin, R. Duballet, Ph. Roux, N. Gaudillière, J. Dirrenberger, and Ph. Morel. Large-scale 3D printing of ultra-high performance concrete – a new processing route for architects and builders. *Materials and Design*, 100:102–109, 2016.

[22] Anon. Standard Die Sets and Hydraulic Presses FAQs. Online. `https://www.pelletpressdiesets.com/pages/die-set-faqs` [Accessed: 26/05/2025].

DOI: 10.13009/EUCASS2025-716

[23] A. Salam, M. Akram, K.A. Shahid, M. Javed, and S.M. Zaidi. Dependence of compressive strength of green compacts on pressure, density and contact area of powder particles. Technical report, Pakistan Inst. of Nuclear Science and Technology, 1994.

[24] Anon. Pressing And Sintering Of Powder Parts. Online. https://thelibraryofmanufacturing.com/pressing_sintering.html [Accessed: 26/05/2025].

[25] M. Kareem, T. Miko, G. Gergely, and Z. Gácsi. A review on the production of 17-4PH parts using press and sinter technology. *Science progress*, 106:368504221146060, 2023.

[26] R. de Oro Calderon, C. Gierl-Mayer, and H. Danninger. Fundamentals of Sintering: Liquid Phase Sintering. In *Encyclopedia of Materials: Metals and Alloys*, pages 481–492. Elsevier, Oxford, 2022.

[27] R.M. German. Chapter Eleven - Mixed Powders and Composites. In *Sintering: from Empirical Observations to Scientific Principles*, pages 355–385. Butterworth-Heinemann, Boston, 2014.

[28] J.D. Kuntz, O.G. Cervantes, A.E. Gash, and Z.A. Munir. Tantalum–tungsten oxide thermite composites prepared by sol–gel synthesis and spark plasma sintering. *Combustion and flame*, 157(8):1566–1571, 2010.

[29] A. Agostinelli. Reactivity characterization of nanometric and activated Al-based thermites. Master's thesis, Politecnico di Milano, 2020.

[30] N. Llorca-Isern and C. Artieda-Guzmán. Metal-based composite powders. In *Advances in Powder Metallurgy*, pages 241–272. Woodhead Publishing, Sawston, 2013.

[31] M.S. Surya and T.V. Nilesh. Synthesis and mechanical behaviour of (Al/SiC) functionally graded material using powder metallurgy technique. *Materials Today: Proceedings*, 18:3501–3506, 2019.

[32] B. Leszczyńska-Madej. The Effect of Sintering Temperature on Microstructure and Properties of Al – SiC Composites / Wpływ Temperatury Spiekania Na Mikrostrukture I Własnosci Kompozytów Al – SiC. *Archives of Metallurgy and Materials*, 58:43–48, 2013.

[33] S. Shankar and D. Apelian. Die soldering: Mechanism of the interface reaction between molten aluminum alloy and tool steel. *Metallurgical and Materials Transactions B*, 33:465–476, 2002.

[34] T. Pieczonka, T. Schubert, S. Baunack, and B. Kieback. Sintering behaviour of aluminium in different atmospheres. In *Proceedings of the Conference 'Sintering '05'*, pages 331–334, 2005.

[35] V.A. Invenson. *Densification of metal powders during sintering*. Springer Science & Business Media, 2012.

[36] R.M. German and A. Bose. Sintering Densification. In *Binder and polymer assisted powder processing*, pages 169 – 191. ASM International, 2020.

[37] J.M. Montes, F.G. Cuevas, and J. Cintas. Porosity Effect on the Electrical Conductivity of Sintered Powder Compacts. *Applied Physics A*, 92:375–380, 2008.

[38] L. Cederle. Reaction of Al/Fe2O3 thermite powders in confined geometries under atmospheric conditions: modelling and experiments. Master's thesis, Politecnico di Milano, 2023.

[39] A. Finazzi. *New concept for sustainable space operations: Thermite-for-Demise (T4D)*. PhD thesis, Politecnico di Milano, 2025.

[40] Anon. Standard Test Methods of Compression Testing of Metallic Materials at Room Temperature, 2025. ASTM Standard E9-19.

[41] Anon. Yield Strength of Aluminum Alloys. Online. https://www.sunrise-metal.com/yield-strength-of-aluminum-alloys/ [Accessed: 12/06/2025].